Azimuthally polarized and unidirectional excitonic emission from deep sub-wavelength transition metal dichalcogenide annular heterostructures

Xingwang Zhang, §, ‡ Wenzhuo Huang, † Chawina De-Eknamkul, § Kedi Wu, \* Meng-qiang Zhao, || Sefaattin Tongay, \* Alan T. Charlie Johnson, ||, ± and Ertugrul Cubukcu §, †, \*

§Department of Nanoengineering, †Department of Electrical and Computer Engineering, University of California, San Diego, La Jolla, California 92093, United States

<sup>‡</sup>Suzhou Institute of Nano-Tech and Nano-Bionics (SINANO), Chinese Academy of Sciences (CAS), Suzhou, Jiangsu 215123, P. R. China

\*School for Engineering of Matter, Transport and Energy, Arizona State University, Tempe, Arizona 85287, United States

Department of Physics and Astronomy, Department of Materials Science and Engineering, University of Pennsylvania, Philadelphia, Pennsylvania 19104, United States

<sup>\*</sup>E-mail: ecubukcu@ucsd.edu

ABSTRACT. Monolayer transition metal dichalcogenides (TMDs) are essential to the scaling down of light-emitting devices to the nanoscale. But the spatial manipulation of their emission at the deep subwavelength scale has remained challenging, limiting their applications in compact directional lighting systems. Here, we present an experimental demonstration of directional and azimuthally polarized excitonic emission from monolayer Tungsten Diselenide (WSe<sub>2</sub>) integrated with deep sub-wavelength Tungsten Disulfide (WS<sub>2</sub>) circular gratings. For such nanoscale heterostructures, the high refractive index of WS<sub>2</sub> enables the existence of guided mode resonances in annular gratings with thicknesses down to the  $\lambda$ /50 length scale. As such, the excitonic photoluminescence from WSe<sub>2</sub> couples into the guided mode resonances of WS<sub>2</sub> nanostructures and radiates as an azimuthally polarized and symmetric beam in the momentum space. Such ringshaped exciton emission at the deep sub-wavelength scale provides more possibilities to miniaturize functional light-emitting devices for azimuthally isotropic illumination.

KEYWORDS. exciton emission, ultrathin, circular gratings, WS<sub>2</sub>, TMD on glass.

Monolayer transition metal dichalcogenides (TMDs) are atomically thin direct band gap semiconductors with tightly bound excitons. 1-3 Due to the quantum confinement effect and associated reduced dielectric screening, monolayer TMDs possess distinctive excitonic emission properties which are normally absent in conventional semiconductors. In addition to this, monolayer TMDs can be freely transferred between different substrates through interlayer Van der Waals forces, forming heterostructures that can potentially serve as ultrathin light sources in various photonic platforms.<sup>4-9</sup> However, the atomically thin nature of the monolayer TMDs also leads to relatively weak light-matter interaction, such that it is challenging for the monolayer TMDs alone to manipulate the 2D excitonic emission properties. In consequence, the 2D excitons in the atomically thin TMDs lack emission directionality, which limits their practical applications in free space communications, <sup>10</sup> optical sensors, <sup>11</sup> optical microscopy, <sup>12</sup> etc. Recent progresses on dielectric photonic crystal (PhC) slabs and metasurfaces have shown that such photonic nanostructures can produce photonic modes with specific angular momentum dispersion, which can be utilized to effectively redistribute the excitonic angular emission of monolayer TMDs.<sup>6, 13</sup> However, due to the low refractive index nature of conventional dielectric materials, these nanostructures usually require a large thickness to support the photonic modes, increasing the thickness of the entire device to hundreds of nanometers despite the atomically thin nature of the monolayer TMDs<sup>6, 13-15</sup>.

For multi-layer TMDs (i.e. TMD thin films), the materials become indirect band gap semiconductors as a result of thickness dependent electronic band structure evolution.<sup>1,16</sup> Though lacking of strong luminescence, TMD thin films still exhibit large exciton oscillator strengths and very high refractive indices (>4) below the exciton resonance, which is desirable for enhancing light-matter interaction in ultrathin photonic nanostructures down to a few atoms thick (Fig. S1).<sup>17</sup>-

Leveraging the high refractive index of excitonic TMDs, we recently demonstrated room temperature exciton-polaritons in Tungsten Disulfide (WS<sub>2</sub>) PhC on glass. In this work, the PhC thickness is pushed down to 10 nm length scale, which is below the typical cut-off thickness for resonators made out of conventional materials while preserving a strong confinement of light.<sup>18</sup>

To this end, we herein present Van der Waals heterostructures consisting of ultrathin WS<sub>2</sub> circular gratings integrated with monolayer Tungsten Diselenide (WSe<sub>2</sub>) to manipulate the polarization and momentum of the WSe<sub>2</sub> exciton emission. Due to the high refractive index of WS<sub>2</sub>, the excitonic emission from WSe<sub>2</sub> is efficiently coupled to the guided mode resonances of the WS<sub>2</sub> circular gratings whose thickness is on the order of  $\lambda$ 50. <sup>18</sup> Meanwhile, the cylindrical symmetry of the WS<sub>2</sub> circular gratings gives rise to an azimuthally isotropic angular momentum dispersion, which redistributes the WSe<sub>2</sub> exciton emission into azimuthally polarized ring-shaped beams with the emission wave vectors propagating on a cone.<sup>21-23</sup> By tuning the angular momentum dispersion of the WS<sub>2</sub> circular gratings, we can tailor the radius and order of the emission ring in the momentum space to achieve unidirectional and high order ring-shaped excitonic emissions. Such azimuthally isotropic excitonic emission fully based on TMDs may have potential applications in ultra-compact vertical emitting light sources with azimuthally isotropic beam properties<sup>24, 25</sup>.

## RESULTS AND DISCUSSION

As schematically shown in Fig. 1a, we constructed the circular gratings with a set of concentric WS<sub>2</sub> rings on silica substrate (see METHODS for more details). The thickness (h) of the WS<sub>2</sub> gratings is in the range of 15 nm $\sim$ 25 nm, which equals to  $\sim$ 1/50 of the operation wavelength ( $\lambda\sim$ 750 nm) (Figs. 1b-c). Due to the high refractive index engendered by excitons, the

WS<sub>2</sub> nanostructures can still support guided mode resonances at the deep subwavelength thickness scale. The cylindrical symmetry nature of concentric rings enables azimuthally isotropic momentum dispersion, which can be used to achieve ring-shaped emission with axisymmetric wave vector distribution. When a point light source is placed in the center of the circular gratings, light is coupled into the guided mode resonances propagating along the radial direction and scattered by the concentric circular Bragg gratings at an angle (see Note S1 in the Supporting Information for more details). <sup>18,19</sup> As such, the wave vectors of the emitted light can be distributed into a cone, forming an ring-shaped beam in the momentum space (i.e. k-space) (Fig. 1a). <sup>19</sup> In addition, by controlling the width (w) and radial period (Λ) of the rings, we can utilize one or several guided mode resonances to generate the first or higher order ring-shaped beams, respectively. Take the WS<sub>2</sub> circular gratings shown in Fig. 1b-c for example, the gratings radial period is 450 nm which only supports the first order guided mode resonance. Therefore, the emission wave vectors for this sample can propagate on a single cone, forming the first order ring-shaped beam (Fig. 1a).

To understand the ring-shaped emission mechanism for 2D excitons, we first studied the momentum dispersion of the WS<sub>2</sub> circular gratings. To this end, we treated the exciton emission of WSe<sub>2</sub> as a broad band point source in the center of the WS<sub>2</sub> circular gratings (Fig. 1a). We then calculated the wavelength dependent far field emission patterns by projecting the near field profiles to the Fourier planes (see METHODS for more details). As can be seen in Fig. 2a, the projection of the light emission in the Fourier plane at  $\lambda$ =820 nm exhibits a single ring-shaped pattern due to the inherent axisymmetric property of the circular gratings structure ( $k_x/k_0$  and  $k_y/k_0$  in the momentum space are related to angles between the emission direction and axes in the real space) (Fig. 1a). In addition to this, due to the highly dispersive guided mode resonances, the ring diameter

on the Fourier plane is wavelength dependent. When the emission wavelength is decreased from  $\lambda$ =820 nm to  $\lambda$ =760 nm, the ring diameter is reduced to zero, leading to the unidirectional emission at the normal direction (Fig. 2a). By further decreasing the emission wavelength to  $\lambda$ =690 nm, a ring-shaped pattern appears again (Fig. 2a). To understand this behavior, we extracted line cuts along k<sub>x</sub>/k<sub>0</sub>=0 from the Fourier images at every wavelength to construct a momentum dispersion map. As can be seen in Fig. 2b, there are two sets of highly dispersive bands with the symmetry about  $k_v/k_0=0$  in the spectral range from  $\lambda=650$  nm to  $\lambda=850$  nm. For a horizontal line cut at a certain wavelength in the momentum dispersion map, the distance between the two peaks corresponds to the diameter of the ring on the Fourier plane. For the upper bands, the diameter of the emission ring in the momentum space increases with the wavelength, and vice versa for the lower bands. At  $\lambda = 760$  nm, the diameter of the ring is reduced to zero, leading to the unidirectional emission case (Fig. 2b). Therefore, by tailoring the momentum dispersion of WS<sub>2</sub> circular gratings, we can achieve both unidirectional and ring-shaped excitonic emissions. Further, we extracted the far field emission patterns of the ring-shaped beam for different polarizations. As shown in Fig. 2c, it turns out that only two arcs of the original ring-shaped patterns parallel to the polarization direction are left in the Fourier planes. This confirms that the output excitonic emission from the WS<sub>2</sub> circular gratings is azimuthally polarized (Fig. 2c).<sup>26</sup>

In our experiments, we first verified our theoretical prediction on the unidirectional 2D exciton emission. We fabricated WS<sub>2</sub> circular gratings with the same parameters as the one simulated in Fig. 2 (see METHODS for more details). To introduce a light source at the center of the circular gratings, we transferred a monolayer WSe<sub>2</sub> onto the sample and used a focused continuous wave (CW) laser ( $\lambda$ =532 nm) to excite the excitonic emission of the monolayer WSe<sub>2</sub> in the center of the circular gratings (Fig. 3a) (see METHODS for more details). The

photoluminescence (PL) spectrum of monolayer WSe<sub>2</sub> has a peak wavelength at  $\lambda$ =750 nm and a full width at half magnitude (FWHM) about 40 nm (Fig. S2), which overlaps with the unidirectional emission spectral region in Fig. 2b. In the WSe<sub>2</sub>/WS<sub>2</sub> heterostructures, the PL of monolayer WSe<sub>2</sub> couples into the guided mode resonance of the WS<sub>2</sub> rings propagating along the radial direction, and then diffracted by the circular gratings to form far field radiation. 19 It should be noted that the imaginary part of refractive index for WS<sub>2</sub> is very low above  $\lambda$ =700 nm, so the optical absorption of WS<sub>2</sub> is negligible (Fig. S1)<sup>18</sup>. To study the angular emission property of the device, we measured the angle-resolved PL spectrum. As shown in Fig. 3b, the PL is primarily enhanced by the guided mode resonance in the normal direction (i.e.  $k_y/k_0=0$ ) at  $\lambda=765$  nm, leading to the red-shift of the PL peak with respect to that of monolayer WSe<sub>2</sub> on glass (i.e.  $\lambda$ =750 nm) (Fig. S3). By taking a line cut at  $\lambda$ =765 nm in Fig. 3b, we can see that the emission divergence is only 6 degrees, indicating a superior unidirectional emission property (Fig. 3d). We note that the unidirectional emission should conserve in the azimuthal direction due to the cylindrical symmetry of our circular gratings. With this in mind, we measured the overall PL far field emission pattern and only a bright light spot can be observed in the center of the Fourier plane (Fig. 3c), indicating the purely unidirectional emission performance without extra azimuthally anisotropic PL residuals (Fig. S4b). In contrast, other 2D exciton emission shaping methods based on PhCs and metasurfaces with square lattice usually suffer from azimuthally anisotropic PL residuals due to additional high order modes.<sup>6, 13</sup>

To further route the 2D exciton emission into an annular shape in the momentum space, we need to shift the momentum dispersion such that the exciton emission wavelength is away from the cross region of the two bands (Figs. 2b and S4). With this in mind, we coated the sample with a layer of polystyrene (PS) (n=1.58). The increase of refractive index in the upper cladding can

red-shift the entire momentum dispersion map, which can be experimentally justified by the angle-resolved PL spectra (Figs. 4a and S5a). Consequently, the original lower bands in Fig. 2b are shifted to the exciton emission spectral region (Fig. 4a). As such, the 2D exciton emission is routed as an azimuthally isotropic annular emission which can be confirmed by the bright ring observed in the Fourier domain (Fig. 4b), indicating the excitonic emission wave vectors propagating into a cone. We also studied the polarization distribution of the ring-shaped beam. To do this, we placed a polarizer in front of the CCD, so only the output light that is polarized along the polarizer can be collected by the CCD (see METHODS for more details). By rotating the polarizer, we find that only two parts of the ring that are parallel to the polarizer can be observed in the CCD (Figs. 4c-4d, Figs. S5c-S5d), which indicates that the polarization distribution of the ring-shaped beam is along the azimuthal direction (i.e. azimuthal polarization). The azimuthal polarization distribution of the ring-shaped beam is resulted from the polarization selection rule of the Bragg scattering of the circular gratings, where only the light that is polarized along the tangent of the WS2 ring can be scattered to the far field.

The single ring we observed in the Fourier domain validated the first order ring-shaped beam emitted by 2D excitons (Fig. 4). We continued to study how to route 2D exciton emission into higher order ring-shaped beam with multiple emission cones. To achieve this, we utilized higher order guided mode resonances of the circular WS<sub>2</sub> gratings. By increasing the radial period ( $\Lambda$ ) from  $\Lambda$ =450 nm to  $\Lambda$ =900 nm, the angular momentum dispersion of the circular WS<sub>2</sub> gratings can be red-shifted so that both the first and second order guided mode resonances overlap with the WSe<sub>2</sub> emission spectrum, enabling bi-directional axisymmetric exciton emission (Fig. S6). To show the exciton emission shaping using these guided mode resonances, we measured angle-resolved PL spectrum, in which we observed two exciton emission bands with the symmetry about

 $k_y/k_0=0$  (Fig. 5a). To study the azimuthal symmetry of the emission bands, we measured the far field emission pattern. As shown in Fig. 5b, we achieved dual ring-shaped emission patterns of the WSe<sub>2</sub> excitons, in which the outer and inner annuli correspond to the first and the second order modes, respectively. In addition, the diameter of the ring can be tuned by shifting the angular momentum dispersion of the circular WS<sub>2</sub> gratings. To this end, we replaced the air cladding of the gratings with a polymer coating (PMMA, n=1.48). The large refractive index increase in the upper cladding can red-shift the dispersion curves by ~50 nm (Fig. S6). Consequently, the WSe<sub>2</sub> PL spectrum now overlaps with the second order mode around  $k_y/k_0=0$  and the first order mode around  $k_y/k_0=0.8$ . As an experimental verification, we measured the angle-resolved PL spectrum and the far field emission pattern. As can be seen in Fig. 5c-d, the inner ring shrinks to a single spot while the outer ring is enlarged as a result of the red-shift of the angular momentum dispersion.

## CONCLUSION

In summary, we experimentally demonstrated the ring-shaped excitonic emission from transition metal dichalcogenides heterostructures, which composed of a monolayer WSe<sub>2</sub> integrated with WS<sub>2</sub> circular gratings with the thickness down to  $\lambda$ /50. The axisymmetric nature of the ultrathin circular gratings enables the uniformity of the angular momentum dispersion in the azimuthal direction to shape the exciton emission of the integrated monolayer WSe<sub>2</sub>. In our experiments, both the unidirectional and ring-shaped exciton emission with azimuthal polarization have been realized by utilizing the different radial guided mode resonances of the WS<sub>2</sub> circular gratings. We believe that our work can potentially enable new techniques for exploring next-generation highly directional light-emitting devices with the emerging 2D semiconductors and beam steering systems with deep sub-wavelength thin nanostructures (Fig. S7).

### **METHODS**

**Monolayer WSe<sub>2</sub> growth.** Monolayer WSe<sub>2</sub> flakes were grown on a SiO<sub>2</sub>/Si substrate by chemical vapor deposition (CVD). First, a mixed solution of 1% sodium cholate and 1.5 mM ammonium heptatungstate was spin-coated onto the substrate. The substrate was then placed in the center of a CVD tube furnace and 150 mg of selenium was placed 13 cm upstream from the substrate. Growth occurred at the atmospheric pressure in a flow of 350 sccm of N<sub>2</sub> and 15 sccm of H<sub>2</sub> at 750 °C.

**Device Fabrication.** The ultrathin WS<sub>2</sub> film was first mechanically exfoliated from bulk WS<sub>2</sub> crystals, and then transferred onto a silica substrate. After that, the chip was spin-coated with PMMA, and then patterned with nanostructures by electron beam lithography. Finally, the nanostructure patterns were transferred from PMMA to WS<sub>2</sub> by Inductively Coupled Plasma - Reactive Ion Etching (ICP-RIE). To construct heterogenous nanostructures, monolayer WSe<sub>2</sub> flakes were first grown on a 300 nm SiO<sub>2</sub>/Si substrate by chemical vapor deposition (CVD), and then transferred onto WS<sub>2</sub> nanostructures.

Optical Measurement. Light from a continuous wave (CW) laser ( $\lambda$ =532 nm) was focused on the monolayer WSe<sub>2</sub> at the center of WS<sub>2</sub> circular gratings by a 100X objective (NA=0.9). To measure the far field emission patterns, the rear focal plane of the objective was projected onto a cooled charge-coupled device (CCD) camera by a Fourier lens. To measure the angle-resolved PL spectra, the far field emission was dispersed by a spectrometer and imaged on the CCD camera, in which the horizontal axis displays the emission wavelength and the vertical axis indicates the emission angle.

Numerical Simulation. Three-dimensional (3D) Finite-difference time-domain method

(FDTD) was used to simulate the far field emission patterns and angular dispersion with a

commercially available software (Lumerical). In the simulation, a broad band point light source

was placed in the center of the WS<sub>2</sub> circular gratings, and a 2D monitor was placed on top of the

device to record the near field and then calculated the far field projection. Perfect matched layers

were used in all the boundaries of the device.

ASSOCIATED CONTENT

**Supporting Information.** 

The Supporting Information is available free of charge at https://pubs.acs.org/doi/

The complex refractive index of WS<sub>2</sub>; Photoluminescence and far field emission pattern of

monolayer WSe<sub>2</sub> on glass; Simulation results for unidirectional and ring-shaped exciton emission.

Experiment results for ring-shaped beam steering; Theoretical analysis of guided-mode resonance

in circular gratings.

**AUTHOR INFORMATION** 

**Corresponding Author** 

\*E-mail: ecubukcu@ucsd.edu.

Notes

The authors declare no competing financial interest.

ACKNOWLEDGMENT

12

This work was supported by NSF under the NSF 2-DARE Program (EFMA-1542879). This work was performed in part at the San Diego Nanotechnology Infrastructure (SDNI) of University of California, San Diego (UCSD), a member of the National Nanotechnology Coordinated Infrastructure (NNCI), which is supported by the National Science Foundation (Grant ECCS-1542148).

#### REFERENCES

- 1. Mak, K. F.; Lee, C.; Hone, J.; Shan, J.; Heinz, T. F., Atomically thin MoS2: a new direct-gap semiconductor. *Phys. Rev. Lett.* **2010**, *105* (13), 136805.
- 2. Li, Y.; Chernikov, A.; Zhang, X.; Rigosi, A.; Hill, H. M.; van der Zande, A. M.; Chenet, D. A.; Shih, E.-M.; Hone, J.; Heinz, T. F., Measurement of the optical dielectric function of monolayer transition-metal dichalcogenides: MoS2, MoSe2, WS2, and WSe2. *Phys. Rev. B* **2014**, *90* (20), 205422.
- 3. Yu, Y.; Yu, Y.; Xu, C.; Cai, Y.-Q.; Su, L.; Zhang, Y.; Zhang, Y.-W.; Gundogdu, K.; Cao, L., Engineering Substrate Interactions for High Luminescence Efficiency of Transition-Metal Dichalcogenide Monolayers. *Adv. Funct. Mater.* **2016**, *26* (26), 4733-4739.
- 4. Zhang, Y. J.; Oka, T.; Suzuki, R.; Ye, J. T.; Iwasa, Y., Electrically switchable chiral light-emitting transistor. *Science* **2014**, *344* (6185), 725-8.
- 5. Baugher, B. W.; Churchill, H. O.; Yang, Y.; Jarillo-Herrero, P., Optoelectronic devices based on electrically tunable p-n diodes in a monolayer dichalcogenide. *Nat. Nanotechnol.* **2014**, *9* (4), 262-7.
- 6. Zhang, X.; Choi, S.; Wang, D.; Naylor, C. H.; Johnson, A. T. C.; Cubukcu, E., Unidirectional Doubly Enhanced MoS2 Emission via Photonic Fano Resonances. *Nano Lett.* **2017**, *17* (11), 6715-6720.
- 7. Lee, B.; Park, J.; Han, G. H.; Ee, H. S.; Naylor, C. H.; Liu, W.; Johnson, A. T.; Agarwal, R., Fano Resonance and Spectrally Modified Photoluminescence Enhancement in Monolayer MoS2 Integrated with Plasmonic Nanoantenna Array. *Nano Lett.* **2015**, *15* (5), 3646-53.
- 8. Palacios, E.; Park, S.; Lauhon, L.; Aydin, K., Identifying Excitation and Emission Rate Contributions to Plasmon-Enhanced Photoluminescence from Monolayer MoS2 Using a Tapered Gold Nanoantenna. *ACS Photonics* **2017**, *4* (7), 1602-1606.
- 9. Mahmood, F.; Alpichshev, Z.; Lee, Y. H.; Kong, J.; Gedik, N., Observation of Exciton-Exciton Interaction Mediated Valley Depolarization in Monolayer MoSe2. *Nano Lett.* **2018**, *18* (1), 223-228.
- 10. Karunatilaka, D.; Zafar, F.; Kalavally, V.; Parthiban, R., LED Based Indoor Visible Light Communications: State of the Art. *IEEE Commun. Surv. Tutor.* **2015**, *17* (3), 1649-1678.
- 11. Prabowo, B. A.; Purwidyantri, A.; Liu, K. C., Surface Plasmon Resonance Optical Sensor: A Review on Light Source Technology. *Biosensors* **2018**, *8* (3), 80.
- 12. Borglin, J.; Wang, D.; Durr, N. J.; Hanstorp, D.; Ben-Yakar, A.; Ericson, M. B., Annular Beam Shaping in Multiphoton Microscopy to Reduce Out-of-Focus Background. *Int. J. Spectrosc.* **2017**, *2017*, 1-10.

- 13. Huang, W.; De-Eknamkul, C.; Zhang, X.; Leewong, E.; Zhao, M.-Q.; Johnson, A. T. C.; Cubukcu, E., Monolayer Excitonic Emission for Imaging Spatial Dispersion of Photonic Crystals. *ACS Photonics* **2019**, *6* (9), 2312-2319.
- 14. Gan, X.; Gao, Y.; Fai Mak, K.; Yao, X.; Shiue, R. J.; van der Zande, A.; Trusheim, M. E.; Hatami, F.; Heinz, T. F.; Hone, J.; Englund, D., Controlling the spontaneous emission rate of monolayer MoS2 in a photonic crystal nanocavity. *Appl Phys Lett* **2013**, *103* (18), 181119.
- 15. Galfsky, T.; Sun, Z.; Considine, C. R.; Chou, C. T.; Ko, W. C.; Lee, Y. H.; Narimanov, E. E.; Menon, V. M., Broadband Enhancement of Spontaneous Emission in Two-Dimensional Semiconductors Using Photonic Hypercrystals. *Nano Lett* **2016**, *16* (8), 4940-5.
- 16. Kuc, A.; Zibouche, N.; Heine, T., Influence of quantum confinement on the electronic structure of the transition metal sulfide TS2. *Phys. Rev. B* **2011**, *83* (24), 245213.
- 17. Beal, A. R.; Liang, W. Y.; Hughes, H. P., Kramers-Kronig analysis of the reflectivity spectra of 3R-WS2 and 2H-WSe2. *J. Phys. C* **1976**, *9*, 2449-57.
- 18. Zhang, X.; Zhang, X.; Huang, W.; Wu, K.; Zhao, M.; Charlie Johnson, A. T.; Tongay, S.; Cubukcu, E., Ultrathin WS2 on Glass Photonic Crystal for Self Resonant Exciton Polaritonics. *Adv. Opt. Mater.* **2020**, *8* (7), 1901988.
- 19. Zhang, X.; De-Eknamkul, C.; Gu, J.; Boehmke, A. L.; Menon, V. M.; Khurgin, J.; Cubukcu, E., Guiding of visible photons at the angstrom thickness limit. *Nat. Nanotechnol.* **2019**, *14* (9), 844-850.
- 20. Liu, W.; Wang, Y.; Zheng, B.; Hwang, M.; Ji, Z.; Liu, G.; Li, Z.; Sorger, V. J.; Pan, A.; Agarwal, R., Observation and Active Control of a Collective Polariton Mode and Polaritonic Band Gap in Few-Layer WS2 Strongly Coupled with Plasmonic Lattices. *Nano Lett.* **2020**, *20* (1), 790-798.
- 21. Fedotowsky, A.; Lehovec, K., Far field diffraction patterns of circular gratings. *Appl. Opt.* **1974**, *13* (11), 2638-42.
- 22. Su, M. Y.; Mirin, R. P., Enhanced light extraction from circular Bragg grating coupled microcavities. *Appl. Phys. Lett.* **2006**, *89* (3), 033105.
- 23. Li, Z.; Alici, K. B.; Caglayan, H.; Ozbay, E., Generation of an axially asymmetric Bessel-like beam from a metallic subwavelength aperture. *Phys. Rev. Lett.* **2009**, *102* (14), 143901.
- 24. Sun, X.; Yariv, A., Modal properties and modal control in vertically emitting annular Bragg lasers. *Opt Express* **2007**, *15* (25), 17323-33.
- 25. Erdogan, T.; King, O.; Wicks, G. W.; Hall, D. G.; Anderson, E. H.; Rooks, M. J., Circularly symmetric operation of a concentric circle grating, surface emitting, AlGaAs/GaAs quantum well semiconductor laser. *Appl. Phys. Lett.* **1992**, *60* (16), 1921-1923.
- 26. Doerr, C. R.; Buhl, L. L., Circular grating coupler for creating focused azimuthally and radially polarized beams. *Opt. Lett.* **2011**, *36* (7), 1209-11.

## **FIGURES**

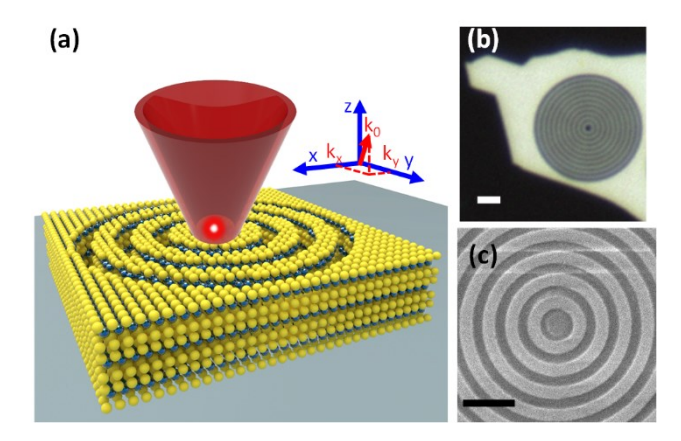


Figure 1. Device structure. (a) Schematic drawing of ultrathin WS<sub>2</sub> circular gratings on a silica substrate. The yellow and blue hard spheres represent the S and W atoms, respectively. In this configuration, the WS<sub>2</sub> circular gratings of deep subwavelength thickness can shape the emission of a point light source (red sphere) into an azimuthally symmetric beam in the far radiation field. Inset: Free space photon momentum  $k_0$  and the in-plane components  $k_x$  and  $k_y$  with respect to the Cartesian coordinate system. The optical microscopy (b) and scanning electron microscopy (c) images (top view) of the WS<sub>2</sub> circular gratings. For this sample, radial period  $\Lambda = 450$  nm, WS<sub>2</sub> ring width w = 250 nm, and thickness h = 25 nm. The scale bars in panel (b) and (c) are 2  $\mu$ m and 500 nm, respectively.

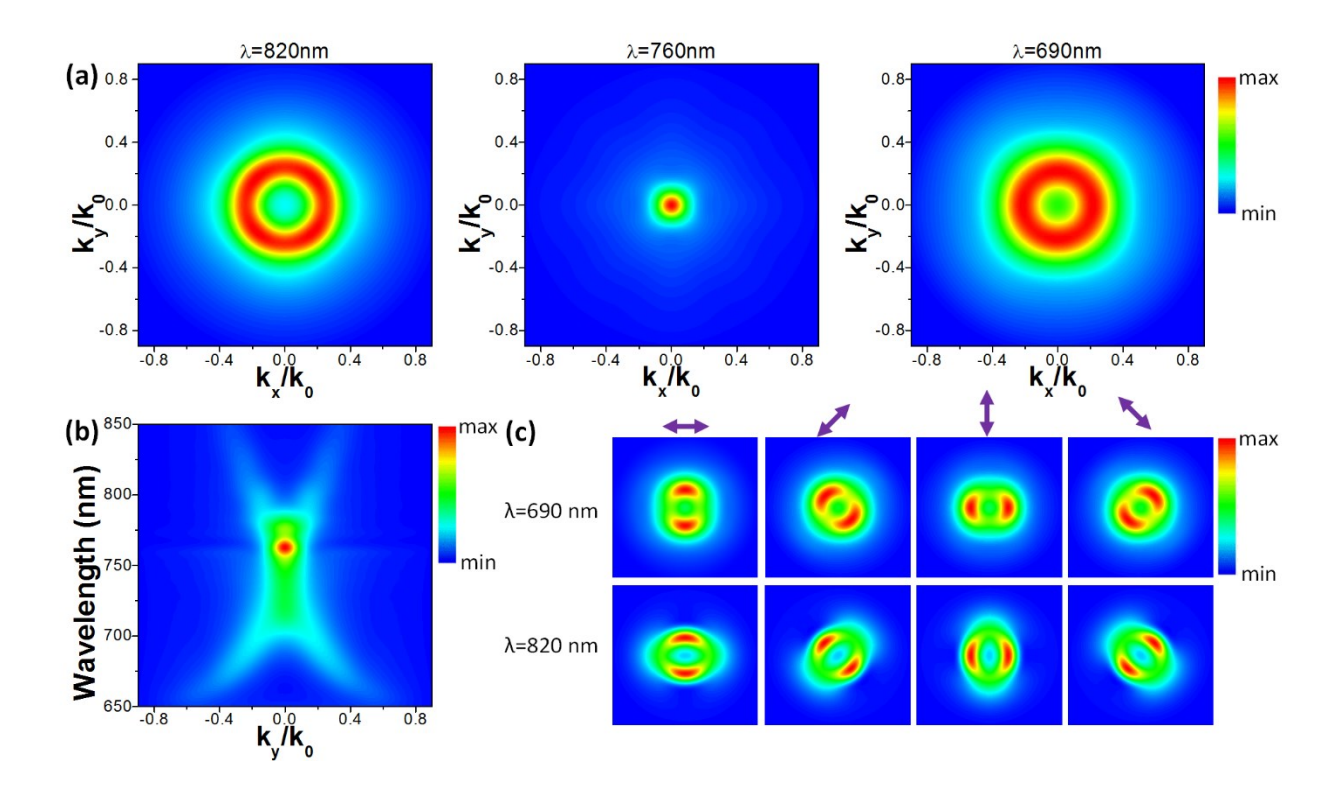


Figure 2. Far-field emission properties of dipoles placed on WS<sub>2</sub> circular gratings. (a) The calculated far field emission patterns for a point dipole in the center of a WS<sub>2</sub> circular gratings at  $\lambda$ =820 nm (left), 760 nm (middle), 690 nm (right), respectively. For this sample, radial period  $\Lambda$  = 450 nm, WS<sub>2</sub> ring width w = 250 nm, and thickness h =25 nm. At  $\lambda$ = 690 nm and  $\lambda$ = 820 nm, ringshaped beams are obtained in the momentum space, while at  $\lambda$ = 760 nm, unidirectional emission is observed. (b) The calculated angular momentum dispersion for the WS<sub>2</sub> circular gratings. There are two sets of highly dispersive bands between  $\lambda$ =650 nm to  $\lambda$ =850 nm. (c) the calculated far field emission patterns for different polarizations. The inset angles indicate the polarization directions. From left to right columns, the polarization angles are: 0°, 45°, 90° and 135° from the +x direction. The upper and lower rows are the far field emission patterns for  $\lambda$ = 690 nm and  $\lambda$ = 820 nm, respectively.

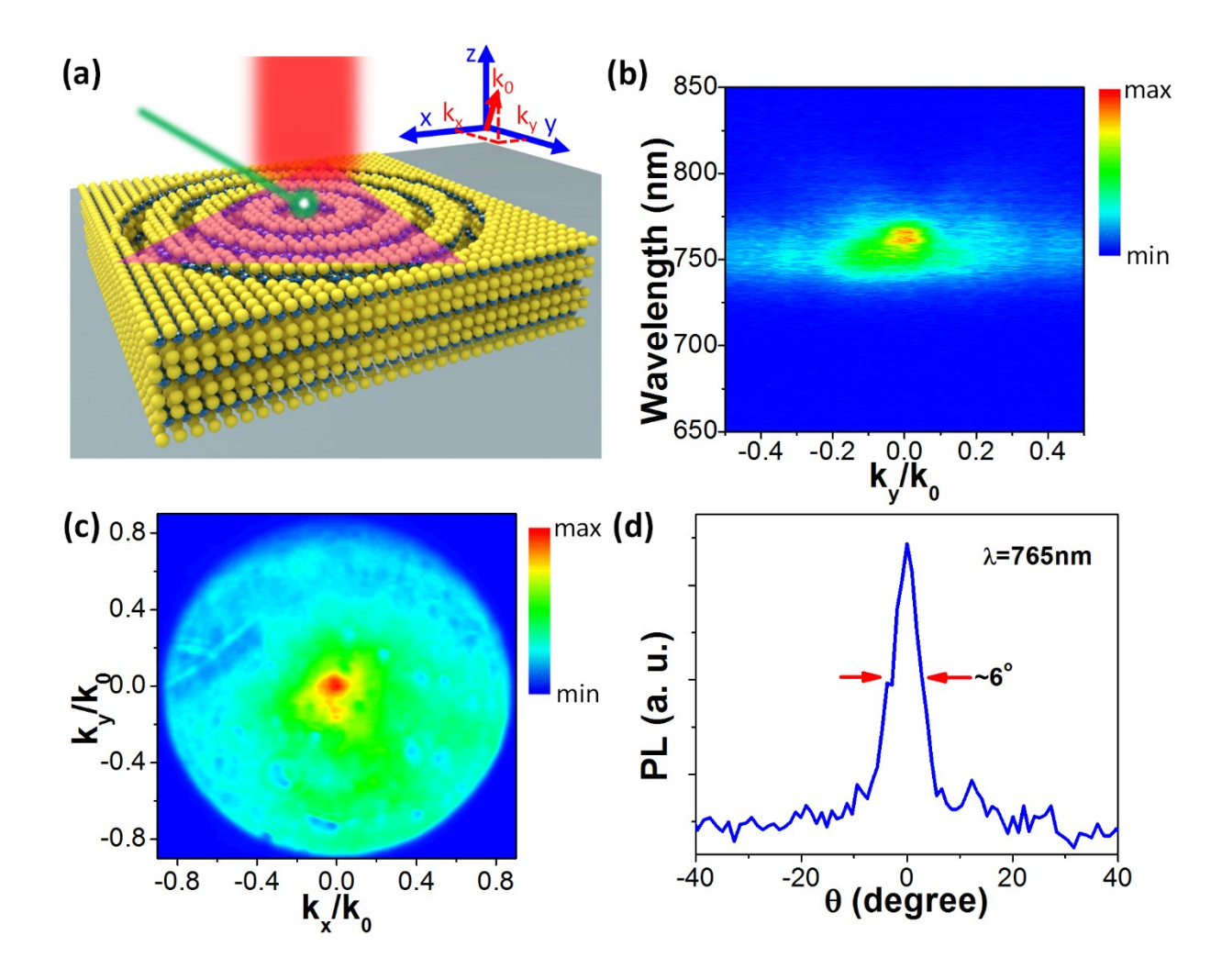
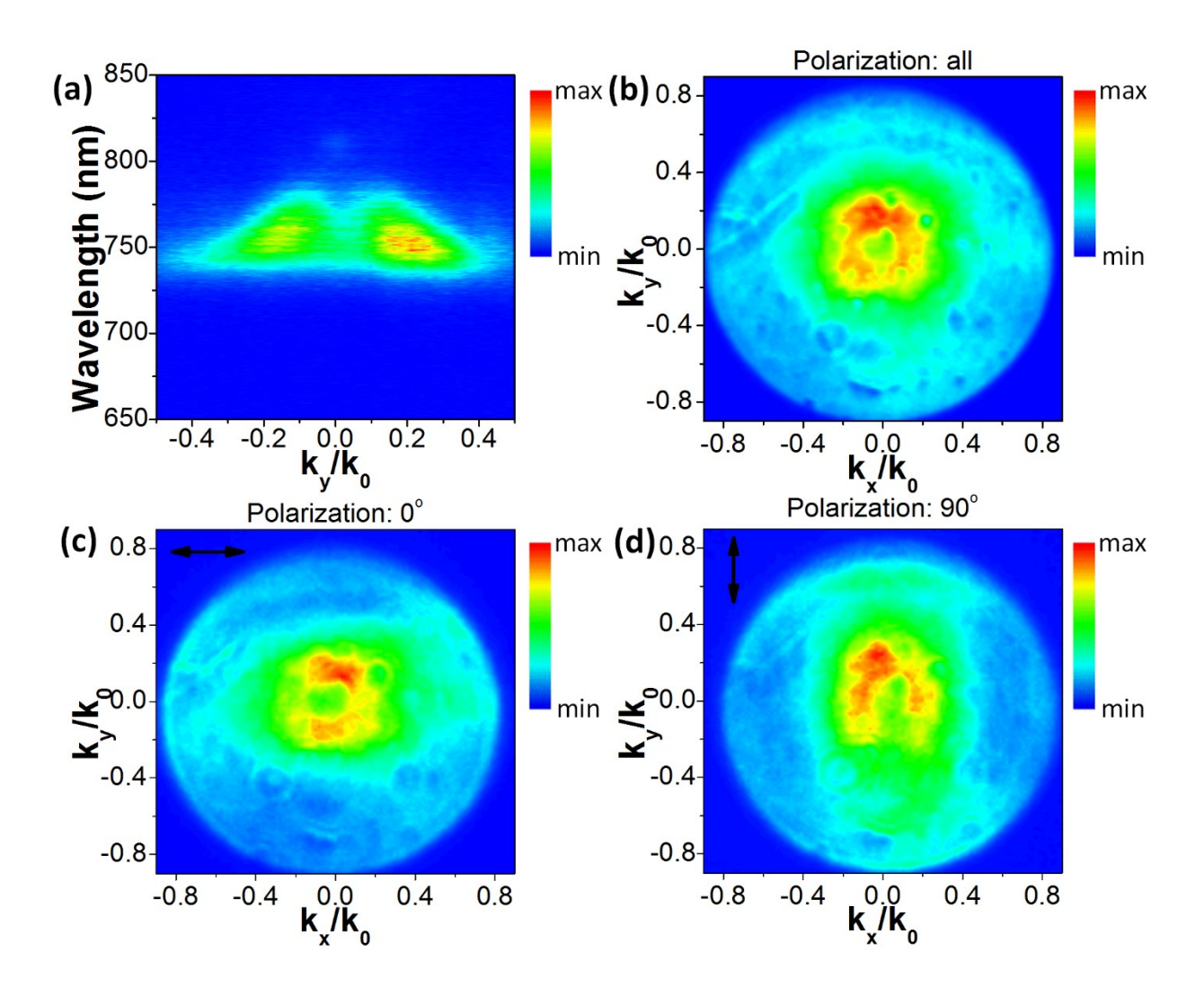


Figure 3. Unidirectional excitonic emission. (a) Schematic drawing of a triangular WSe<sub>2</sub> monolayer on ultrathin WS<sub>2</sub> circular gratings on silica substrate. A continuous wave (CW) green laser ( $\lambda$ =532 nm) is used to excite the WSe<sub>2</sub> excitonic emission in the center of the gratings. The output photoluminescence (PL) is shaped by the gratings and unidirectional emission is realized in the normal direction. Inset: Free space photon momentum k<sub>0</sub> and the in-plane components k<sub>x</sub> and k<sub>y</sub> with respect to the Cartesian coordinate system. (b) The measured angle-resolved PL spectrum shows the PL is mainly routed in the normal direction (i.e. k<sub>y</sub>/k<sub>0</sub>=0) around  $\lambda$ =765 nm. (c) PL far field emission pattern shows the PL is primarily concentrated at k<sub>x</sub>=k<sub>y</sub>=0. (d) The angle dependence of PL at  $\lambda$ =765 nm shows that the divergence angle of PL emission is about 6°.



**Figure 4.** The first order ring-shaped excitonic emission. (a) The measured angle-resolved PL spectrum for the polystyrene (PS) coated device shows the red-shifted momentum dispersion compared with Fig. 3b. (b) PL far field emission pattern shows that the PL is primarily concentrated in a ring in the Fourier plane (i.e. ring-shaped excitonic emission). PL far field emission patterns for the x- (c) and y- (d) polarizations indicate the polarization of the emitted ring-shaped beam is along the tangent of the ring (i.e. azimuthal polarization).

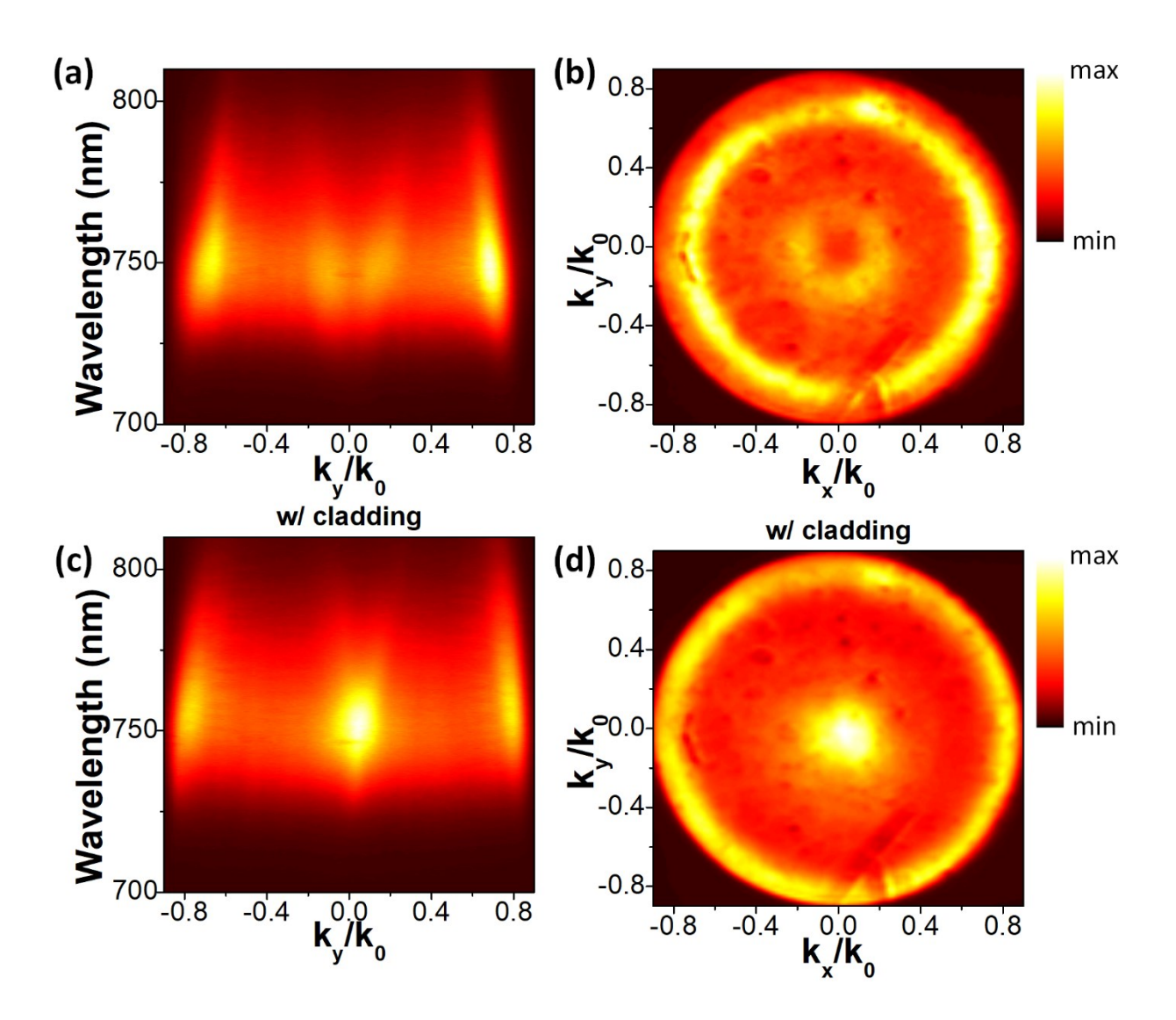
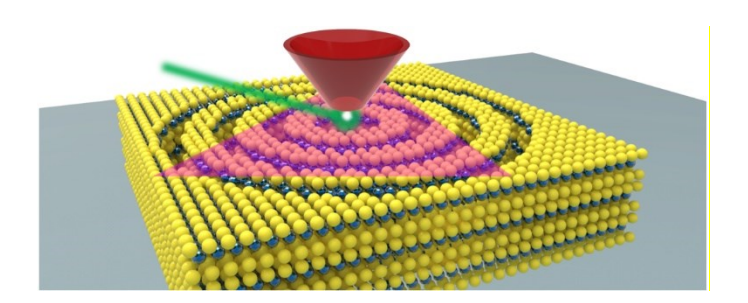


Figure 5. Higher order ring-shaped excitonic emission. The angle-resolved PL spectra for monolayer WSe<sub>2</sub> on an ultrathin WS<sub>2</sub> circular grating with (c) and without (a) PMMA top layer. The PL emission of monolayer WSe<sub>2</sub> is efficiently coupled to two radial guided mode resonances of WS<sub>2</sub> circular gratings. The measured far field emission patterns for monolayer WSe<sub>2</sub> on ultrathin WS<sub>2</sub> annular gratings with air (b) and PMMA (d) top layers. Two concentric rings are observed for the former case, while a single ring with a central spot is observed for the latter case. For this sample, the radial period  $\Lambda = 900$  nm, WS<sub>2</sub> ring width w = 600 nm, and thickness h = 15 nm.

# For Table of Contents Use Only



Manuscript title: Azimuthally polarized and unidirectional excitonic emission from deep subwavelength transition metal dichalcogenide annular heterostructures

Names of authors: Xingwang Zhang, Wenzhuo Huang, Chawina De-Eknamkul, Kedi Wu, Mengqiang Zhao, Sefaattin Tongay, Alan T. Charlie Johnson, and Ertugrul Cubukcu

**Brief synopsis:** We present Van der Waals heterostructures consisting of ultrathin WS<sub>2</sub> circular gratings integrated with monolayer Tungsten Diselenide (WSe<sub>2</sub>) to manipulate the polarization and momentum of the WSe<sub>2</sub> exciton emission.